# Automatic Optical-to-SAR Image Registration by Iterative Line Extraction and Voronoi Integrated Spectral Point Matching

Haigang Sui, Chuan Xu, Junyi Liu, and Feng Hua

***Abstract*—Automatic optical-to-SAR image registration is considered as a challenging problem because of the inconsistency of radiometric and geometric properties. Feature-based methods have proven to be effective; however, common features are difficult to extract and match, and the robustness of those methods strongly depends on feature extraction results. In this paper, a new method based on iterative line extraction and Voronoi integrated spectral point matching is developed. The core idea consists of three aspects: 1) An iterative procedure that combines line segment extraction and line intersections matching is proposed to avoid registration failure caused by poor feature extraction. 2) A multilevel strategy of coarse-to-fine registration is presented. The coarse registration aims to preserve main linear structures while reducing data redundancy, thus providing robust feature matching results for fine registration. 3) Voronoi diagram is introduced into spectral point matching to further enhance the matching accuracy between two sets of line intersection. Experimental results show that the proposed method improves the matching performance. Compared with previous methods, the proposed algorithm can effectively and robustly generate sufficient reliable point pairs and provide accurate registration.**

***Index Terms*—Iterative line extraction, multiscale, optical-to-SAR image registration, Voronoi integrated spectral point matching (VSPM), Voronoi polygons.**

## I. Introduction

IMAGE registration is the process of overlaying two or more images of a given scene that are captured at different times, from different viewpoints, and/or by different sensors [1]. High accuracy has long being pursued, as it fundamentally determines the accuracy for image fusion and change detection [2]. It has been recognized that the complementary use of optical and SAR data can be meaningful [3], [4]: Optical data have good interpretability, but they are easily affected by atmosphere condition, whereas SAR data are able to deliver information at all day and night, but they suffer from serious intrinsic speckle noise. Therefore, information accurately extracted from both data sources would further expand our capability on Earth observation.

However, automatic registration of optical-to-SAR images is considered challenging because of the following [5], [6].

- Different geometric properties. The side-looking and measuring distances mode of a SAR sensor would cause a series of geometrical distortions known as foreshortening, layover, and shadow, which do not exist in the corresponding optical image.
- Different radiometric characteristics. SAR instruments are active remote sensing system in the field of microwaves, whereas optical instruments are passive system in the field of visible and near infrared. The brightness values may change significantly due to the variation in imaging conditions.
- Strong speckle noises by SAR sensors. Sensor and environmental noises make the feature extraction difficult in SAR images and hinder the effort of identifying common features between optical and SAR images.

There are two major categories of optical-to-SAR images registration methods: intensity-based and feature-based methods. Widely used intensity-based methods include mutual information [7]–[11], normalized cross-correlation coefficient [12], and cross-cumulative residual entropy [13]. However, these methods may lead to local extrema and high computation load [14], [15]. Moreover, when geometric distortion between the images to be registered is significant, these methods can be ineffective [16]. In contrast, feature-based methods have proven to be more suitable for multisensory image registration [17]–[20], as image features are less sensitive to illumination, reflectance, and geometry inconsistency. Points [21], lines [22]–[27], and regions [28] are among the most commonly used image features. In contrast, linear and region features can be more easily distinguished and matched than distinct points for multisensor image registration [29]. However, as conjugate region features in an image pair are not always sufficiently available, linear features could be a good alternative for its interpretability and stability in detection process.

Typical linear features can be contours [24], [25], edges [19], [22], [23], and straight line segments [26], [27]. However, well-identifiable features are not as easy to be detected in SAR images as in optical images due to the strong speckle noise. Traditional line-segments-based methods usually utilize line segments as matching primitives [26], [27]. However, it

Manuscript received January 21, 2014; revised July 8, 2014, November 7, 2014, and March 4, 2015; accepted April 1, 2015. This work was supported in part by the Hi-Tech Research and Development Program of China (863 Program) under Grant 2013AA122301 and in part by the National Basic Research Program of China (973 Program) under Grant 2012CB719906.

The authors are with the State Key Laboratory of Information Engineering in Surveying, Mapping and Remote Sensing, Wuhan University, Wuhan 430079, China (e-mail: xc992002@foxmail.com; 53046034@qq.com; liujunyi_ljy@163.com; huafeng731@gmail.com).

Color versions of one or more of the figures in this paper are available online at http://ieeexplore.ieee.org.

Digital Object Identifier 10.1109/TGRS.2015.2431498

requires a large number of line features for convergence and involves the computation of a "Hough accumulator" [26], and the similarity measure is difficult to define [27]. Straight line segments can be identified by end points, and conjugate line segments do not require being at the same position. Thus, using line intersections as matching primitives can be a better alternative.

Unfortunately, feature correspondence techniques remain unsatisfactory to support this matching alternative [30]–[32]. Spectral point matching (SPM) is considered as one of the most effective methods for point matching. It aims to characterize the global structural properties of related graphs using the eigenvalues and eigenvectors of adjacency matrix [33]. However, its high sensitivity to noise and outliers limits the accuracy. To avoid these problems, Voronoi polygons method is introduced to incorporate the impacts from neighboring points. In addition, angle consistency constraint is used to further guide the correspondence.

On the other hand, iterative feature extraction and matching strategy is adopted to support the registration method. Almost all feature-based registration methods rely on the robustness of feature detection for reliable matching. Although some of them can yield satisfactory registration results, they are only effective for specific images. Due to the variation of illumination, different viewpoints and image qualities, and so on, developing a universal line extraction method could be challenging. As a result, performing feature extraction only once before matching regardless of the image sources usually results in matching failure.

Moreover, extracted features from images may differ a lot in number, length, and location due to the existing differences in optical and SAR images. Isolated line features caused by different details in optical and SAR images can pose great challenge to feature matching. To deal with this issue, a multilevel strategy that provides coarse-to-fine registration is introduced to meet this challenge.

Based on the aforementioned consideration, this paper proposes an automatic optical-to-SAR image registration method based on iterative line extraction and Voronoi integrated SPM. The following tasks are attempted to be achieved in this paper.

1) A new point matching method, which is called Voronoi integrated SPM (VSPM), is proposed to obtain point correspondence among line intersections. The core idea of VSPM is introducing Voronoi polygons into SPM, which combines both local structure and global structure to establish correspondence. Traditional Euclidean distance is replaced by Hausdorff distance between Voronoi polygons to incorporate the impact from neighboring points. Furthermore, angle consistency constraint is used to exclude impossible correspondence.
2) An iterative strategy that involves adaptive parameter adjustment for reextracting and rematching features is presented. Considering the fact that almost all feature-based registration methods rely on feature extraction results, the iterative strategy improves the robustness of feature matching. In addition, all parameters can be automatically and adaptively adjusted in the iterative procedure.
3) A multilevel framework that provides coarse-to-fine registration is proposed. Searching the entire image for feature extraction would cause great challenge to feature matching since the details in the optical and SAR images differ a lot. Thus, coarse registration is implemented at low resolution level to preserve the main spatial structures while eliminating the details, followed by iterated feature extraction and matching. With the help of transformation obtained at the coarse registration, refined registration is implemented at the original images. Obviously, using the coarse-to-fine registration framework can improve the efficiency of the proposed method.

The remainder of this paper is organized as follows. Section II briefly describes the framework of the proposed registration method. Section III illustrates the detail methodology of the iterative line segments extraction strategy and VSPM algorithm. Section IV provides the experiment results. This paper concludes with a summary of major findings and discussion of implication on optical-to-SAR image registration in Section V.

## II. Research Framework

The framework of our proposed method is shown in Fig. 1. Considering the fact that the use of extracted features from the original optical and SAR images is difficult for feature matching due to their significant difference, a coarse-to-fine registration framework is adopted to provide accurate and robust registration.

In the coarse registration procedure, registration based on line intersections is performed to obtain the initial perspective parameters. Then, the so-called VSPM is introduced to find best point correspondences. Furthermore, the matching accuracy is checked to find whether the image pair is well registered or not. If the registration accuracy is not satisfactory, the iterative feature extraction and matching mechanism is triggered to get optimized matching result. In the fine registration procedure, conjugate line segments are judged according to rough deformation acquired at the coarse registration, and tie points are obtained after a robust outlier removal procedure. Thus, a precise estimation of local transformations between the images is obtained.

## III. Methodology

### A. Line Segments Extraction and Preprocessing

The extraction of geometric primitives would strongly influence the ultimate accuracy of image registration. Due to the multiplicative speckle in SAR images, methods that are efficient for optical images do not provide a constant false alarm rate for SAR images. Thus, different extraction measures are required for optical and SAR images.

*1) Optical Images Line Extraction:* Line segment detector (LSD) [34], which aims at detecting straight contours on images, has been applied to extract linear features from remote sensing image. It extracts line segments with relatively low false alarm rate. To this end, LSD is employed to extract line segments from optical images.

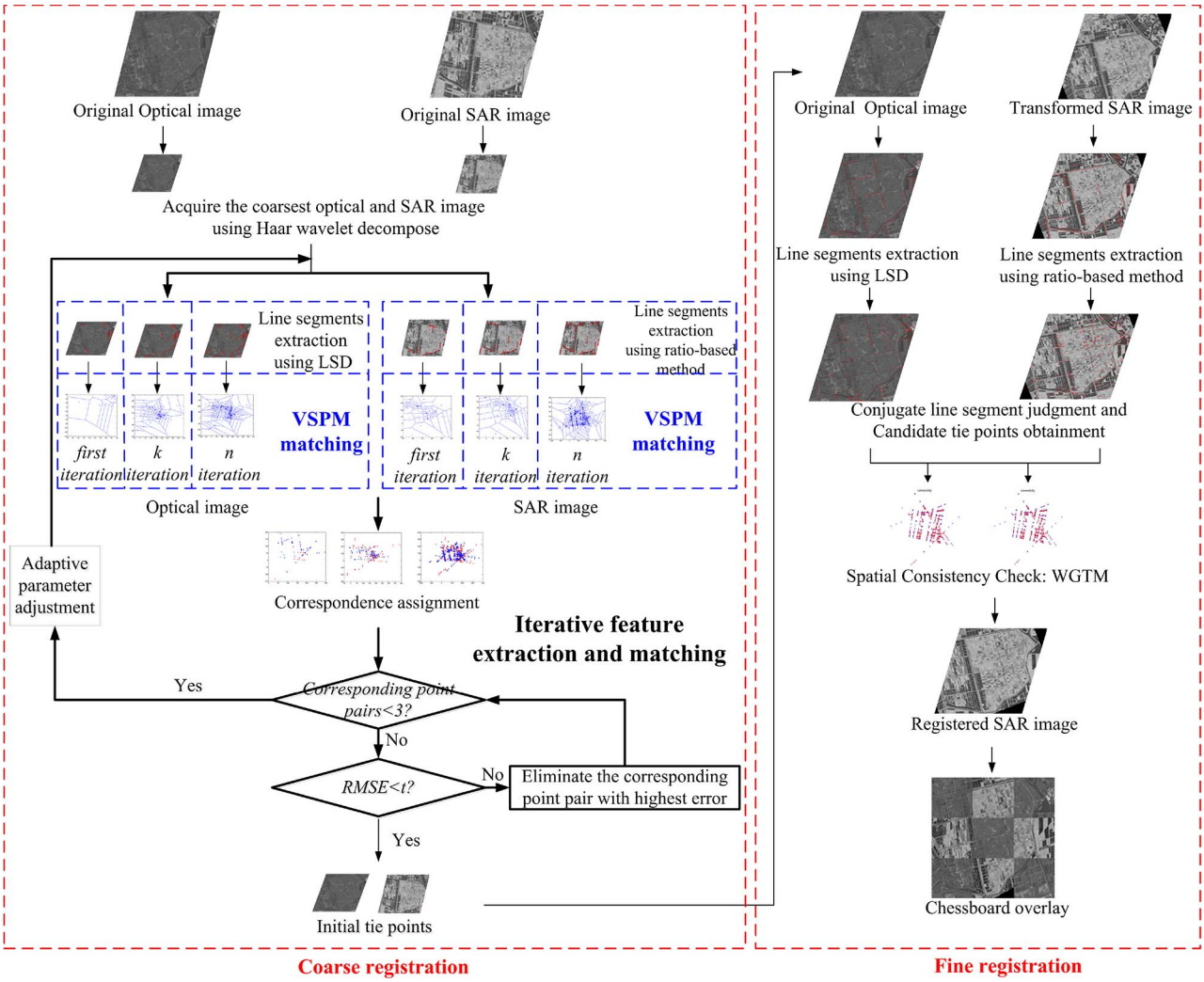


Fig. 1. Framework of the proposed method.

*2) SAR Images Line Extraction:* It is also recognized that speckle noise degrades the SAR image quality [35]. A filtering strategy using a Lee filter [36] is performed. Taking the advantages of its flexible parameter selection, gradually widened spacing between two windows, and good smoothness in local mean estimation, edge detector using Gaussian-gamma-shaped (GGS) bi-windows [37] has shown better performance than traditional rectangle bi-windows for edge detection in SAR images. Then, after extracting edges using the GGS-based method, Hough transform is performed to obtain line segments in SAR images.

*3) Line Segments Preprocessing:* We now present the calculation of intersection points as matching primitives. Extracted line segments often appear fragmented or incomplete. Moreover, because of image quality and downsampling, the terminals of extracted segments may have positioning errors. To reduce the positioning errors, we propose the following two constraints.

The first one is length constraint, considering that long line segments can be more robust. For fragmented line segments, redundancy would be eliminated to preserve the longest line as main structure [see Fig. 2(a)]. For the remaining line segments, the length of each line segments should exceed a given threshold $t_l$. The larger the threshold, the more robust line segments are left for matching primitives generation. It is set to 15 for the image no larger than $256 \times 256$ pixels according to experiments. For larger images, $t_l$ is chosen as $15 \times \lfloor N/256 \rfloor$, where $\lfloor \bullet \rfloor$ is the floor function, and $N$ is the minimum of the width and height of the input image.

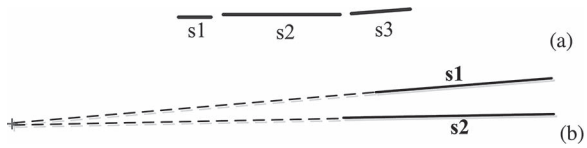


Fig. 2. Line segments preprocessing. (a) Redundant fragmented line segments removal. Suppose that three fragmented line segments s1, s2, and s3 are extracted for an edge. The longer line segment can be more robust; thus, the longest line s2 is preserved, whereas the line segments s1 and s3 are rejected. (b) To avoid intersection produced by two nearly parallel line segments, line segments with an intersection angle less than 10° would not be considered in calculating a feature point.

The second one is angle constraint. If two line segments are nearly parallel, their intersection can be unstable and far away from the real situation [see Fig. 2(b)]. Thus, in our method,

those line segments with intersection angle less than 10° are not considered. Only the line segment pairs satisfying the two constraints would be used to calculate the feature points.

### *B. VSPM Matching*

The spectral method of Shapiro and Brady [38] maps the original 2-D data to a higher dimensional space and captures structural information from the feature points, and thus finds correspondence by performing alignment in the eigenspace. One key point in this idea is to find an appropriate proximity matrix, which reflects the global structure of a given data set. Traditional Euclidean-distance-based proximity matrix is sensitive to local positioning jitters. Moreover, the performance of the method can be even poor in the existence of outliers.

Finding correspondence between two point-sets purely depending on global structure can be ineffective when outliers exist. It is necessary to take the points' local structure into consideration to deal with the ambiguity for point matching. Voronoi diagram, which is a way of dividing space into a number of regions, has two distinct advantages that make it suitable for representing local structure. The first one is the stability. Once a point is inserted or missing, the changes do not affect global stability. The second one is its affine invariance. Distortions caused by deformation do not influence the global topology between Voronoi cells. Thus, we introduce a new point matching method based on the integration of Voronoi polygons and SPM.

In our method, Voronoi polygons [39] are introduced into a spectral graph. Similar with the SPM method, which measures point relationship by Euclidean distance, we measure polygon relationship by Hausdorff distance. Then, the proximity matrix $H$ can be computed as

$$H = [h_{ij}] = \begin{cases} -r_{ij}^2, & i \neq j \\ -\sum\limits_{k \neq i} r_{ik}, & i = j \end{cases} \tag{1}$$

$$rij = e^{-\text{hausdorff}(VPi, VQj)/2\sigma 2} \tag{2}$$

$$\text{hausdorff}(A, B) = \max\left(h(A, B), h(B, A)\right) \tag{3}$$

$$h(A, B) = \max_{a \in A}\left\{\min_{b \in B}\{d(a, b)\}\right\} \tag{4}$$

where $r_{ij}$ is the Gaussian weighted distance between two Voronoi polygons $VP_i$ and $VQ_j$. hausdorff$(A, B)$ is the Hausdorff distance between polygons $A$ and $B$; $a$ and $b$ are the points of polygons $A$ and $B$, respectively. $\sigma$ is a parameter controlling the degree of interaction between points.

Next, the modal structure of point-set $P$ associated with optical line intersection set and point-set $Q$ associated with SAR line intersection set is found by performing eigenvalue decomposition on the proximity matrices $HP$ and $HQ$, i.e.,

$$HP = \text{UEU}^T \tag{5}$$

$$HQ = \text{VDV}^T. \tag{6}$$

The diagonal values of $E$ and $D$ are the eigenvalues of $U$ and $V$ in decreasing order, respectively. The columns of $U$ ($V$, respectively) are eigenvectors of $HP$ ($HQ$, respectively) corresponding to eigenvalues in $E$ ($D$, respectively).

To avoid the problem of eigenvalue multiplicity [40], a perturbation matrix $K$ is added to proximity matrices $HP$ and $HQ$, i.e.,

$$K_1 = U\text{diag}(\delta, \delta^2, \ldots, \delta^m)U^T \tag{7}$$

$$K_2 = V\text{diag}(\xi, \xi^2, \ldots, \xi^m)V^T. \tag{8}$$

$\delta$ and $\zeta$ are independent realizations from a uniform distribution over the interval (0,1). Since their value is very small, a slight perturbation operation still makes the eigenvalues distinct.

To solve the sign ambiguity when computing eigenvectors at the situations $Ax = \lambda x$ and $A(-x) = \lambda(-x)$, a sign correction is performed. For each column $v_i$ in $V$, suppose that each column $u_i$ in $U$ is given, then the corrected sign of $v_i$ is determined as follows:

$$v_i' = \begin{cases} v_i, & \text{if } \|u_i + v_i\| > \|u_i - v_i\| \\ -v_i, & \text{otherwise} \end{cases} \text{for } (1 \leqslant i \leqslant \min(m, n)). \tag{9}$$

According to Shapiro and Brady, the correspondence probabilities are assigned by the smallest modal Euclidean distance. In our method, the angle consistency constraint is used to guide the correspondence. Suppose that two line segments $(L_1^O, L_2^O)$ in the optical image generate the point $P_O$ and $(L_1^S, L_2^S)$ in the SAR image generate the point $P_S$, and the two points are corresponding points. If the angle difference is too large between $(L_1^O, L_2^O)$ and $(L_1^S, L_2^S)$, it is impossible that two points $(P_O, P_S)$ are corresponding points. Then, we quantize the angle consistency constraint as

$$A(P_O, P_S) = \begin{cases} 1, & \text{if } \left|\theta\left(L_1^O, L_2^O\right) - \theta\left(L_1^S, L_2^S\right)\right| < t \\ 0, & \text{otherwise.} \end{cases} \tag{10}$$

$A(P_O, P_S)$ is the possibility for $P_o$ and $P_S$ to be a pair of corresponding points from the angle consistency constraint concept. $t$ is the threshold controlling sensitivity on deformations. For a good match, $\theta(L_1^O, L_2^O)$ must be equal to $\theta(L_1^S, L_2^S)$. However, in practical aspects, if the deviation between the angles lies within the threshold $t$, then the angle consistency constraint is satisfied. It can be set to 5° according to experiments. Then, final similarity $Z$ between $P$ and $Q$ can be measured by computing the affinity between their corresponding spectral and the angle consistency constraint, i.e.,

$$Z = A(UV'^T). \tag{11}$$

$V'$ denotes the revised matrix of $V$. If $Z_{ij}$ is the greatest value in both row $i$ and column $j$, then we considered the $i$th point in $U$ and the $j$th point in $V$ to be a match pair.

It should be noted that the point matching process is performed on the coarse registration at low-resolution image. In the proposed method, outliers come from isolated lines in two images. At the low-resolution image, extracted line features are salient structures in images. Thus, only few isolated lines can be detected in the optical and SAR images. Then, few outliers exist in the point matching process. This can be one of the main reasons that we adopt the multiscale registration strategy.

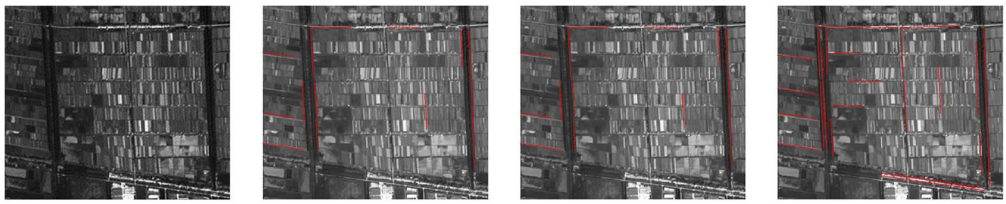

(a) (b) (c) (d)

Fig. 3. Line segment extraction using LSD with different $\tau$. (a) Tested optical image. (b) $\tau = 22.5$. (c) $\tau = 30$. (d) $\tau = 45$.

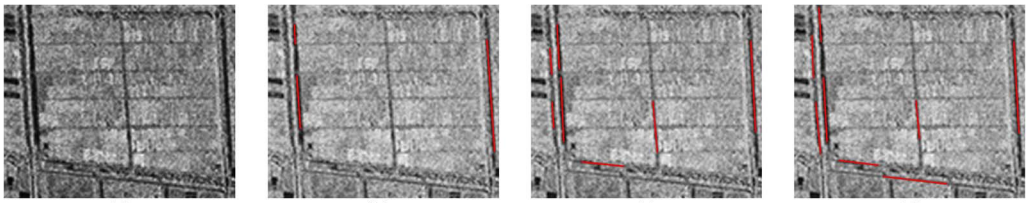

(a) (b) (c) (d)

Fig. 4. Edge detection using GGS biwindows with different $\beta$. (a) Tested SAR image. (b) $\beta = 1.5$. (c) $\beta = 2$. (d) $\beta = 2.5$.

Once all corresponding point pairs are detected, their matching accuracies are checked by the global consistency method based on affine transformation model. Those with highest errors are rejected one by one until the root-mean-square error (RMSE) is achieving $\text{rmse}_{\text{Affine}} < 1$ pixel. Otherwise, the iteration stops if the remaining corresponding point pairs are three, with $\text{rmse}_{\text{Affine}} > 1$ pixel.

### C. Iterative Strategy

There are many existing feature-based matching methods for automatic registration in multisource images. However, one-time feature extraction algorithms may significantly limit the matching accuracy due to poor extraction results [41]–[43]. Thus, a "reextracting" and "rematching" strategy is introduced to improve matching performance, which mainly involves adaptive parameter adjustment for line extraction.

The basic idea of LSD is to find out line segment candidates and then validate or not each line segment based on the information in the line-support region. In the line segment candidates searching procedure, each line-support region starts with one pixel and the region angle set to the level-line angle at that pixel. Then, the pixels adjacent to the region are tested; the ones with level-line orientation equal to the region angle up to a certain precision are added to the region. The process is repeated until no new point can be added. There are three parameters involved in LSD: $\rho$, which is the threshold on the gradient magnitude, and pixels with small gradient are not considered in the search of line-support regions; $\tau$, which is the angle tolerance, used in the search for line-support regions; and $\varepsilon$, which is the detection parameter restricting the number of false alarms in the validation. As shown in [34], $\varepsilon$ is not a critical parameter; $\rho$ determines whether the pixel is used in the construction of line-support regions; however, it depends on $\tau$. It has been recognized that, in critical-size regions or when noise is strong, the parameter $\tau$ is particularly important. There is no theory behind this parameter value. However, a small $\tau$ value leads to an overpartition of line segments, and a large $\tau$ value results in large regions. The proposed value 22.5° corresponds to eight different angle bins, and it is supported by the results on thousands of images [34]. Here, an optical image with different $\tau$ (22.5°, 30°, 45°) is tested. In Fig. 3, we can see that, as $\tau$ increases, more line segments can be detected.

For line segment detection in SAR images, the two main steps are edge detection and Hough transform. The edge detection result is fundamental and critical for SAR images with multiplicative speckle. Ratio-based method with GGS biwindows [37] is adopted as edge detector, which can sufficiently reduce false edge pixels in the vicinity of true edges. The horizontal biwindow consists of two 2-D window functions:

$$W_U(x,y) = \frac{|y|^{\alpha-1}}{\sqrt{2\pi}\sigma_x\Gamma(\alpha)\beta^\alpha}\exp\left(-\left(\frac{x^2}{2\sigma_x^2}+\frac{|y|}{\beta}\right)\right), \quad y\geqslant 0$$
$$W_L(x,y) = \frac{|y|^{\alpha-1}}{\sqrt{2\pi}\sigma_x\Gamma(\alpha)\beta^\alpha}\exp\left(-\left(\frac{x^2}{2\sigma_x^2}+\frac{|y|}{\beta}\right)\right), \quad y\leqslant 0. \tag{12}$$

The detection performance depends on three parameters: $\sigma_x$, which controls the window length, and $\alpha$ and $\beta$ ($\alpha > 1, \beta > 0$), which control the window width and the spacing of the two windows. The spacing between two windows in a biwindow is necessary for edge detection, since an appropriate spacing can assure that the two windows support the homogenous regions on the two sides of the edge. Given the rectangle bi-window with length $l_f$, width $w_f$, and spacing $d_f$, the relationship between a GGS bi-window and a rectangle bi-window is

$$l_f = 2\sqrt{\pi}\sigma_x \quad w_f = \frac{\Gamma^2(\alpha)2^{2\alpha-1}\beta}{\Gamma(2\alpha-1)}. \tag{13}$$

Different from the rectangle bi-window with a constant spacing $d_f$, the spacing in a GGS bi-window gradually widens along its central line, which is affected by $\alpha$ and $\beta$ jointly. The size of the detection region is chosen to contain enough pixels to respect the line structures. Similar with [37], the window length is set to $6.5/\sqrt{\pi}$. Setting $\alpha = 3$ fixed, $\beta = 1.5$, 2, and 2.5 (It is equivalent to having the window widths of 8, 10, and 13 respectively.) are tested for a real SAR scenario. As shown in Fig. 4, as $\beta$ increases, more line segments are extracted.

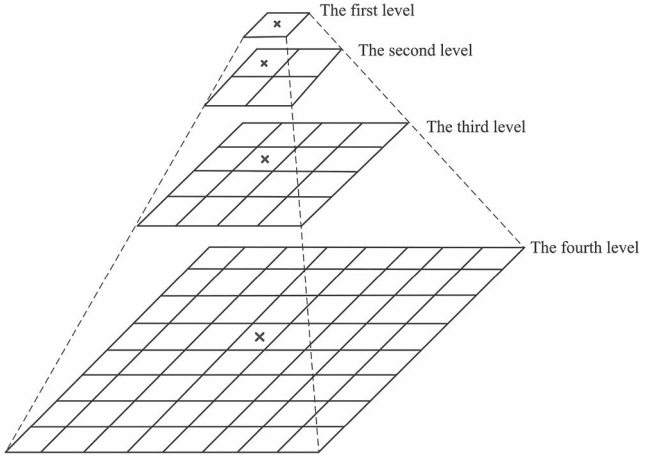


Fig. 5. Corresponding point mapping relationship between the low resolution level and the high resolution level. The crosspoint is obtained by VSPM used to be projected to the original image.

In our proposed iterative mechanism, the initial value for $\tau$ is set to 22.5, as recommended in [34], and the initial value for $\beta$ is set to 1.5, as recommended in [37], respectively. If the coarse registration using initial values for feature extraction and VSPM is not satisfactory, the iterative feature extraction and matching is started. The iterative procedure enhances the coarse registration accuracy by adjusting feature extraction parameters. The adjustment is based on extracted features in both the optical and SAR images. The parameter will increase when features extracted from either optical image or SAR image are insufficient with the increasing interval of 7.5° to $\tau$ for the optical image and 0.5 to $\beta$ for the SAR image. If the iteration number is achieved to a given iteration value and the following feature rematching still fails, then the registration is considered as failure.

### *D. Fine Registration*

Having those corresponding points obtained at low resolution level, we first project them to the original images. If the point in the downsampled image is found to be $(x, y)$, then the projected point in the original image can be simplified as $2^L \times (x, y) - 2^{L-1}$, where $L$ is the downsampling level (see Fig. 5). An affine model is used as the transformation model between the optical and SAR images. Based on the projected points in the original images, initial affine transformation parameters can be obtained for guiding conjugate line segments judgment.

With the help of corresponding points obtained at low resolution level, the original SAR image can be transformed, and then, line segments extracted at high resolution level are matched based on a specific matching cost function, and candidate tie points can be obtained. Line intersections between conjugate line segments can be used to estimate transformations based on the second polynomial transformation. The equation for second-order transformation function is given by

$$\begin{aligned} X &= a_0 + a_1 x + a_2 y + a_3 xy + a_4 x^2 + a_5 y^2 \\ Y &= b_0 + b_1 x + b_2 y + b_3 xy + b_4 x^2 + b_5 y^2. \end{aligned} \tag{14}$$

In order to efficiently find conjugate line segments, a specific matching cost function, which represents the matching quality between two line segments, is developed. The matching cost function relies on the angular difference between the segments and on the distance from the center of one of them to the other straight line and is defined as [44]

$$C_{\gamma\theta}(s_i, o_j) = \frac{1}{\sqrt{2}} \left\{ \left[ \frac{d_\gamma(s_i, o_j)}{d_{\gamma\max}} \right]^2 + \left[ \frac{d_\theta(s_i, o_j)}{d_{\theta\max}} \right]^2 \right\}^{1/2} \tag{15}$$

where $d_\gamma(s_i, o_j)$ is the distance from the center of $o_j$ to the line defined by $s_i$; $d_\theta(s_i, o_j)$ is the angular difference between $o_j$ and $s_i$; and $d_{\gamma\max}$ and $d_{\theta\max}$ are the maximum allowed values for $d_\gamma$ and $d_\theta$, respectively, and are used for normalization purposes. The resulting normalized distance will be 0 if the $i$th line segment in the optical image and the $j$th line segment in the SAR image is matching. If the distance is greater than 1, it is assumed that the segments do not match. For the images of this paper, the following values have been used for normalization:

$$d_{\gamma\max} = 5 \text{ pixels} \quad d_{\theta\max} = 3^\circ.$$

Suppose that $m$ line segments are extracted in the original optical image and $n$ line segments are extracted in the transformed SAR image. For each line segment $s_i$ in the SAR image, the line segments in the optical image, which have similar slope with $s_i$, are selected to calculate the matching cost using (15). If there is no selected line segment or all the matching costs are greater than 1, the current line segment is considered as isolated. Otherwise, the line segment with the minimum matching cost is considered to be matched with $s_i$.

For the input optical and SAR images, two sets of features can be obtained by intersecting the conjugate line segments. Theoretically, these line intersections are very likely paired. However, due to the significant differences between the optical and SAR images, there may exist distortions between the line intersections. In order to avoid wrong pairs in the line intersections, weighted graph transformation matching [45] is used to check and remove those wrong pairs, and the remaining corresponding points are used to produce the final registered images.

### *E. Effect of Line Extraction Quality on Registration Accuracy*

Due to different geometries of SAR and optical images, the extracted lines for a given feature in the scene may differ in position and orientation. Since line intersection is used as matching primitive, the final registration accuracy can be affected by the quality of the line segments detected. In this paper, two aspects are considered to help reduce the effect of line extraction error on the registration accuracy. First, length and angle constraints are set to each line pair to generate robust point features. Second, a matching accuracy checking procedure is applied to both coarse and fine registration steps to exclude unreliable matching pairs.

TABLE I
EXPERIMENT DATA SETS

| Test Data | Data Description | | |
|---|---|---|---|
| | Optical image | SAR image | Study area description |
| Dataset1 | Sensor: UAV<br>Resolution: 3m<br>Date: \<br>Size: 460*400 | Sensor : UAV<br>Resolution: 3m<br>Date: \<br>Size: 577*599 | The image pair is UAV images with the same resolution acquired over Albuquerque International Airport, United States. Tested images are downloaded from: http://www.sandia.gov/RADAR/imageryku.html. The selected data have significant radiation differences; Meanwhile, the SAR image is artificially rotated by 30 degree. |
| Dataset2 | Sensor: UAV<br>Resolution: 0.5m<br>Date: April, 2012<br>Size: 4140*3240 | Sensor: UAV<br>Resolution: 1m<br>Date: April, 2012<br>Size: 2272*1636 | The study area is with Mianyang City, Sichuan Province, China. Tested images are high resolution UAV images in suburb area. Similarly, the two images have significant radiation differences. Furthermore, the quality of the optical image degrades by cloud, which aggravates the registration difficulty. |
| Dataset3 | Sensor: SPOT<br>Resolution: 2.5m<br>Date: Mar. , 2011<br>Size: 1686*1521 | Sensor: TerraSAR-X (VV polarization)<br>Resolution: 1m<br>Date: Aug., 2012<br>Size: 3285*2238 | The study area is with Wuhan City, Hubei Province, China. A number of farmland exists in the study area. There is a seasonal difference between the two images, which shows radiation changes in the farmland. What is more, the SAR image suffers speckle noise seriously. |
| Dataset4 | Sensor: QuickBird<br>Resolution: 0.61m<br>Date: Sept., 2012<br>Size: 3634*3333 | Sensor: Cosmo<br>Resolution: 1m<br>Date: May, 2008<br>Size: 1868*1351 | The study area is with Dujiangyan, Sichuan province, China. Tested images are high resolution satellite images in suburb area. Linear features are distinct and rich in the two images. However, the brightness of the two images is not correlated, and there are also differences due to images being captured with a difference of four years. |
| Dataset5 | Sensor: TM B5<br>Resolution: 30m<br>Date: May, 2003<br>Size: 386*356 | Sensor: HJ-1C<br>Resolution: 5m<br>Date: Dec., 2012<br>Size: 2243*2328 | The study area is with Wuhan City, Hubei Province, China. Tested images are medium-low resolution satellite images in urban area. The scaling difference between tested images reaches six times and the time interval is nine years. |

## IV. EXPERIMENTAL RESULTS

Here, five sets of experiments (see Table I) are designed to evaluate the proposed approach and compared with previous methods. The first two sets exemplify the importance of the point correspondence, whereas the others aim to demonstrate the necessity of iterative strategy. Finally, all sets are carried out to provide comparative results.

### A. Point Matching Methods Comparison

To evaluate the effectiveness of point correspondence, we compared the proposed approach (VSPM) with the methods SPM [42] and SPM plus angle consistency constraint (ACC).

For Data Set 1, two images are in similar spatial resolution. The SAR image is manually rotated by 30° counterclockwise. As shown in Fig. 6(a), 16 line segments from the optical image (left) and 14 line segments from the SAR image (right) are extracted. Isolated line segments are highlighted in green, whereas segments with corresponding ones are in yellow. Eighty-seven points from the optical image and 71 points from the SAR image are regarded as matching primitives in the coarse registration. The matching performance of different point matching algorithms is shown in Fig. 6(b)–(d). Outliers and local positioning jitters are mainly caused by isolated line intersections and line segments location offsets. As shown in Fig. 6(d), a lot of matches are false, although many matching

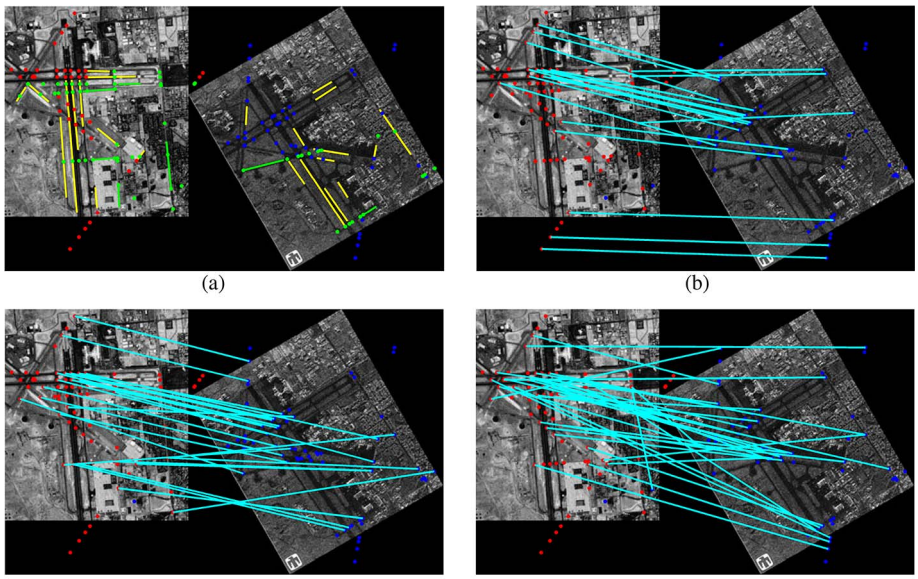

Fig. 6. Point matching results for Data Set 1. (a) Line segments extraction and intersection generation. (b) Point correspondence using VSPM. (c) Point correspondence using SPM+ACC. (d) Point correspondence using SPM.

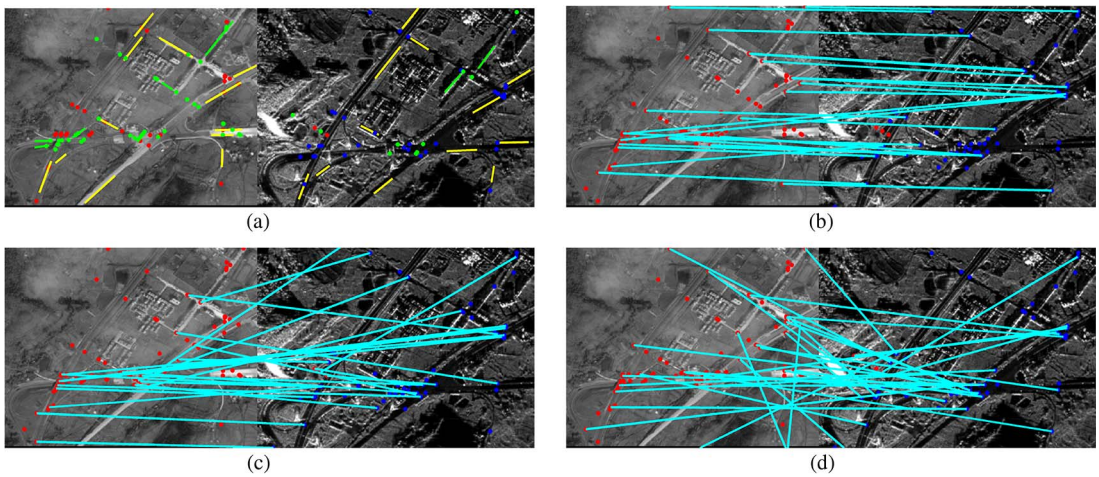

Fig. 7. Point matching results for Data Set 2. (a) Line segments extraction and intersection generation. (b) Point correspondence using VSPM. (c) Point correspondence using SPM+ACC. (d) Point correspondence using SPM.

pairs are obtained using the SPM method. In Fig. 6(c), correct matches increase, although there are still a lot of false matches. In Fig. 6(b), the matched pairs are almost correct, although the matched number decreases. The matching results demonstrate that the proposed VSPM improves the matching performance.

For Data Set 2 (see Fig. 7), two images have different spatial resolutions. The extracted line segments from the optical and SAR images are 17 and 14, respectively. Eighty-four points from the optical image and 50 points from the SAR image are used as matching primitives. The aforementioned comparisons indicate the advantage of the proposed point matching method.

Table II summarizes the experiment results from Data Set 1 and Data Set 2. The following are observed. 1) The introduction of Voronoi polygons is beneficial for validating the primitive candidate, with a significant increase in matching ratio. 2) The angle consistency constraint is helpful for reducing obvious correspondence errors. The angle consistency constraint can be used as a guide to exclude those impossible matching points.

TABLE II
POINT MATCHING RESULTS USING DIFFERENT METHODS

| Image Pair | Matching results | VSPM | SPM+ACC | SPM |
|---|---|---|---|---|
| Dataset 1 | Initial matches | 21 | 26 | 31 |
| | Correct matches | 16 | 12 | 8 |
| | Matching ratio | 76.19% | 46.15% | 25.80% |
| Dataset 2 | Initial matches | 25 | 30 | 34 |
| | Correct matches | 20 | 16 | 9 |
| | Matching ratio | 80.00% | 53.33% | 26.47% |
| Dataset 3 | Initial matches | 20 | 28 | 35 |
| | Correct matches | 15 | 13 | 9 |
| | Matching ratio | 75.00% | 46.42% | 25.71% |
| Dataset 4 | Initial matches | 18 | 25 | 30 |
| | Correct matches | 14 | 12 | 9 |
| | Matching ratio | 77.78% | 48.00% | 30.00% |
| Dataset 5 | Initial matches | 22 | 28 | 35 |
| | Correct matches | 16 | 12 | 10 |
| | Matching ratio | 72.73% | 42.86% | 28.57% |

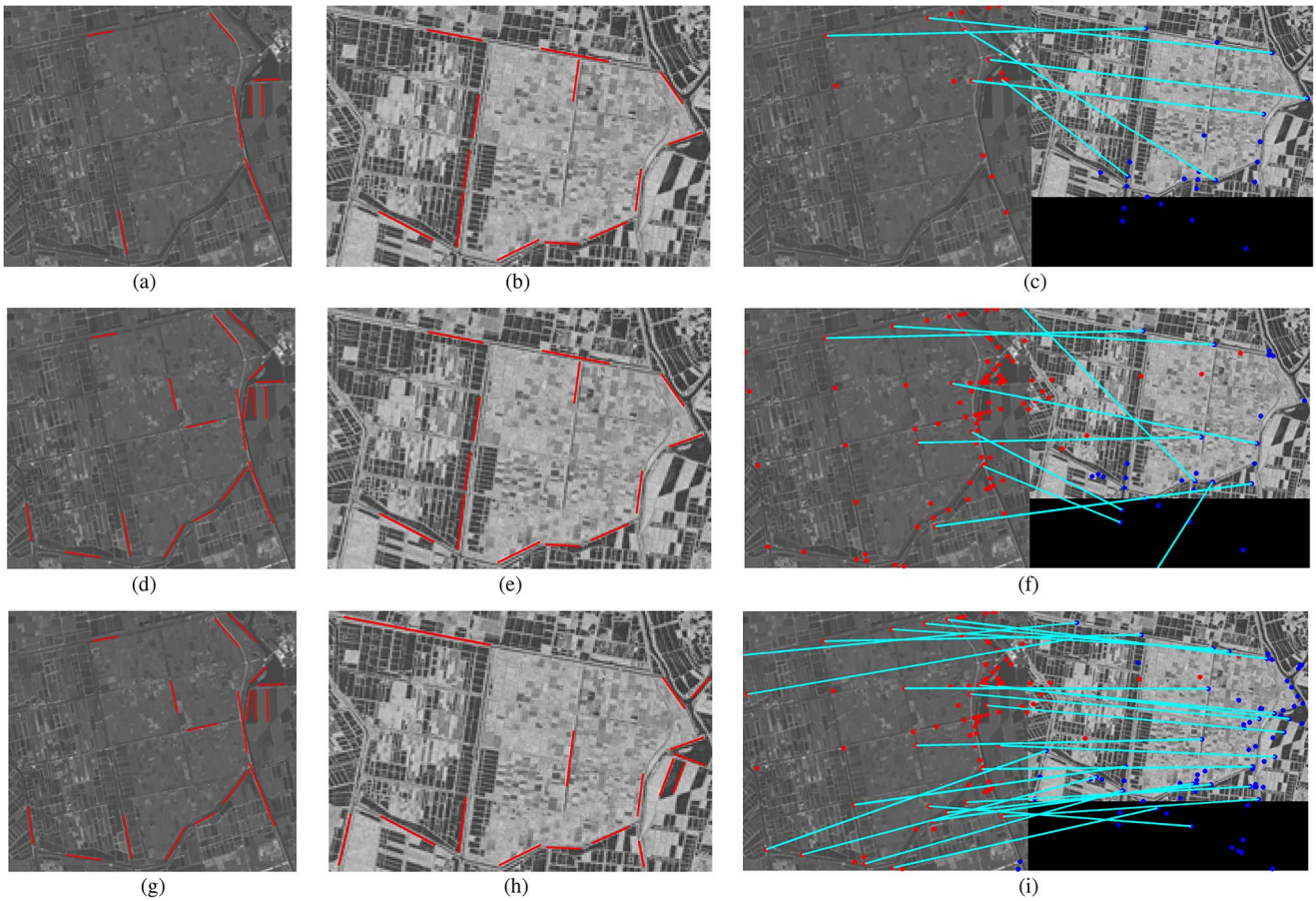


Fig. 8. Iterative line segments extraction and matching for Data Set 3. (a) $\tau = 22.5$. (b) $\beta = 1.5$. (c) First iteration. (d) $\tau = 30$. (e) $\beta = 1.5$. (f) Second iteration. (g) $\tau = 30$. (h) $\beta = 2$. (i) Third iteration.

This is an advantage of choosing straight line segments to provide matching primitives. 3) The proposed method may obtain less corresponding points than SPM. Due to the Voronoi polygons having taken the neighborhood point's impact into account, when the point have too many outliers around, the current point may fail to find the corresponding point. On the other hand, in the SPM method, points are independent and free from the surrounding points. However, in the coarse registration step, the more important thing is to provide robust correct matched points for guiding the fine registration step.

### *B. Iterative Line Segment Extraction and Matching*

Three sets of experiments are designed to evaluate iterative strategy for registration. The first and second sets of images are in high spatial resolution. The third set of images is in medium spatial resolution.

For Data Set 3 (see Fig. 8), the optical and SAR images are downsampled to the resolution of 211 $\times$ 191 and 206 $\times$ 140 pixels. In the first iteration, most extracted line segments in the optical and SAR images are isolated. Six pairs of corresponding points are obtained with three wrong pairs. At the second iteration, the SAR image is fixed; line segments are reextracted in the optical image with the control parameter increasing by 7.5. However, the optical image extracts much more line segments than the SAR image; the number of matching primitives from the optical image is 133, and that from the SAR image is 38. The matching result is not desirable under this condition. At the third iteration, the optical image is fixed; line segments are reextracted in the SAR image with the control parameters increasing by 0.5. Most extracted line segments are not isolated, and the matching primitive for SAR image increases to 120. Finally, 20 pairs of corresponding points are obtained, with 15 correct pairs.

On the other hand, in Date Set 4 (see Fig. 9), salient line features are difficult to extract from the low-resolution SAR image due to reduced contrast after downsampling. At the first extraction procedure, only features along river, which shows a great contrast with the ground in the image, are detected. At the second extraction procedure, extraction performance has been improved; however, the coarse registration still failed. At the third extraction procedure, real corresponding line segments are much more than outliers in the detected candidates. There are 17 pairs of corresponding points obtained, among which 15 pairs are correct.

For Data Set 5 (see Fig. 10), in the first iteration, 14 line segments are detected in the optical image, and 25 segments are detected in the SAR image. The numbers of line intersections for point matching are 82 and 250 from the optical and SAR images, respectively. The outliers in the point-set from SAR

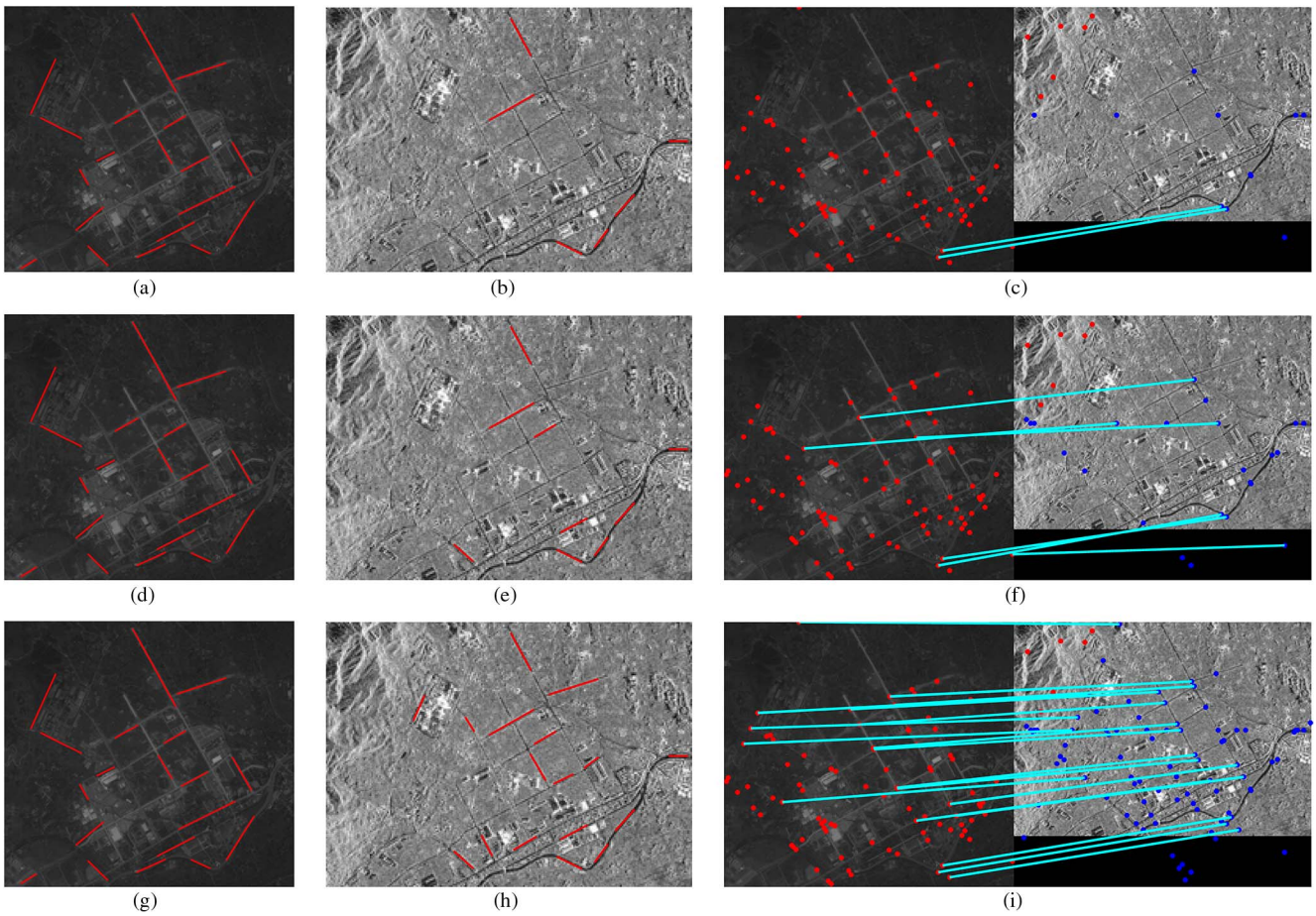


Fig. 9. Iterative line segments detection and matching for Data Set 4. (a) $\tau = 22.5$. (b) $\beta = 1.5$. (c) First iteration. (d) $\tau = 22.5$. (e) $\beta = 2$. (f) Second iteration. (g) $\tau = 22.5$. (h) $\beta = 2.5$. (i) Third iteration.

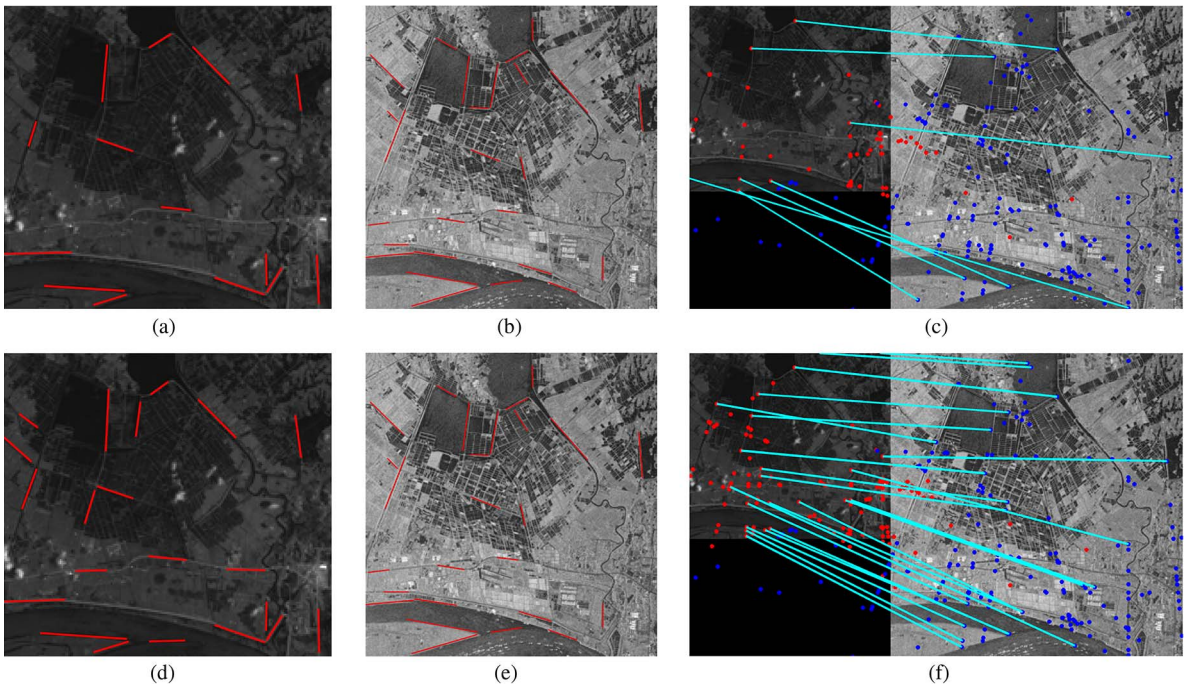


Fig. 10. Iterative line segments detection and matching for Data Set 5. (a) $\tau = 22.5$. (b) $\beta = 1.5$. (c) First iteration. (d) $\tau = 30$. (e) $\beta = 1.5$. (f) Third iteration.

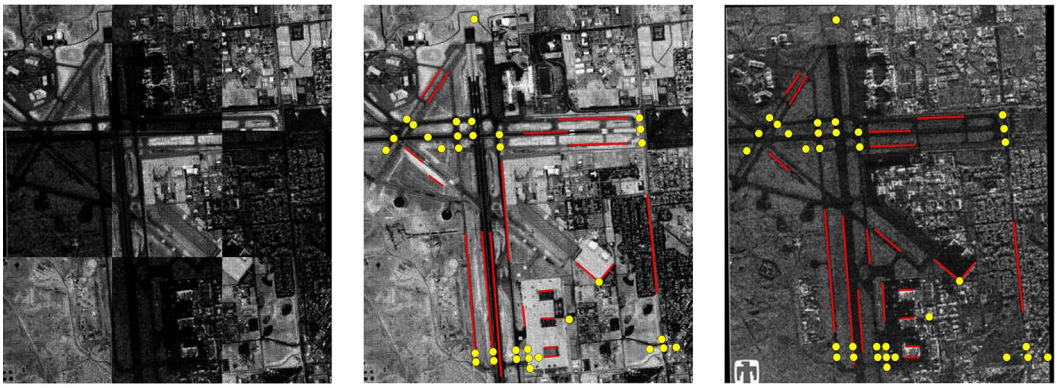

(a) (b) (c)

Fig. 11. (a) Chessboard overlay for Data Set 1. (b) Final control points in the optical image. (c) Final control points in the SAR image.

(a) (b) (c)

Fig. 12. (a) Chessboard overlay for Data Set 2. (b) Final control points in the optical image. (c) Final control points in the SAR image.

image are too many that VSPM only obtained seven matching pairs. In the second iteration, 21 line segments are detected from the optical image, and 25 line segments are detected from the SAR image. The number of matched point pairs is 22, in which 16 point pairs are used as control points for coarse transformation after using global consistency checking.

In general, feature-based methods often require sophisticated image processing for feature extraction and depend on the robustness of feature detection for reliable matching [46]. Although the effectiveness of feature matching is crucial to the accuracy of image registration, the matching performance is affected by feature extraction results. Well-extracted features alleviate the matching challenge. However, performing feature extraction and matching only once would not be effective to most image pairs (as for the three tested images); thus, iterative feature extraction and matching is necessary to provide robust matching.

### C. Algorithms Comparisons

To evaluate our proposed registration method, three kinds of popular methods are chosen to be compared with. The first is based on the mutual information (MI) [7], which is a widely used area-based method for optical and SAR image registration. The improved scale invariant feature transform (SIFT) [21] is considered as the second method of comparison, whereas modified iterated hough transform (MIHT) [26] is the third considered method. Because three sets of the test images have insufficient regional feature (Data Set 1, Data Set 2, Data Set 4), which would lead to regional-based method failure, we do not adopt any regional-based methods for comparison. The images are processed on a computer with an Intel Core 2 540 3.07-GHz processor and 8.0 GB of physical memory, using Microsoft Visual C++. The comparison is divided into two parts. The first part is a direct comparison with other methods. The second part is a degraded comparison of the proposed method. Since the proposed method benefits from the well-known effects of the coarse-to-fine approach such as less outliers and raw disparity estimates, the comparison at the fine level is also implemented for fairness.

*Direct Comparison:* MI and improved SIFT fail to match the five image pairs. For Data Set 1, only seven pairs of keypoints are extracted using improved SIFT, and none of the matched pairs is correct. For the other data sets, no corresponding keypoint pairs can be detected. The MIHT method can register Data Set 1 and Data Set 2. However, the matching accuracy is 15.6436 pixels for Data Set 1 and 21.9424 pixels for Data Set 2. For the proposed method, all data sets are successfully registered. The test results (chessboard overlay, final set of line segments, and keypoints) are presented in Figs. 11–15. A quantitative result of the tested images is listed in Table III. In addition to the widely used measure of root mean square, some other proposed measures are also evaluated [47]. Considering that the other methods cannot successfully register these images, the quantitative results of these methods are not reported.

(a) (b) (c)

Fig. 13. (a) Chessboard overlay for Data Set 3. (b) Final control points in the optical image. (c) Final control in the SAR image.

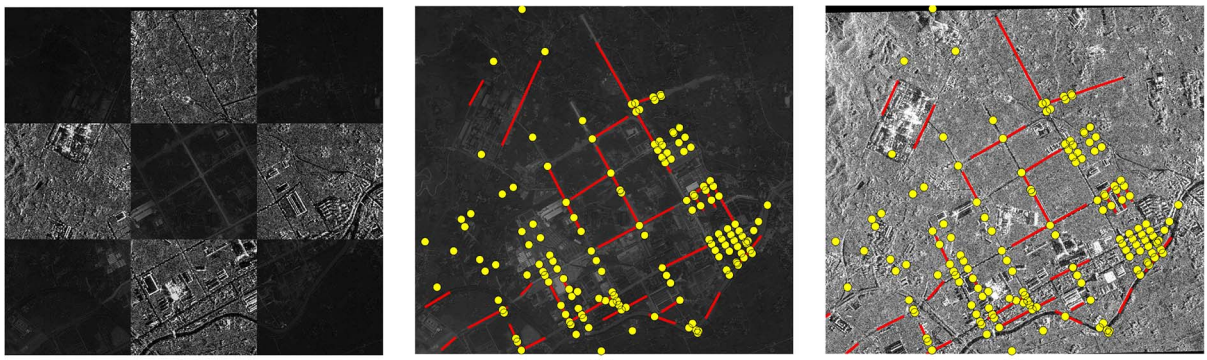

(a) (b) (c)

Fig. 14. (a) Chessboard overlay for Data Set 4. (b) Final conjugate line segments in the optical image. (c) Final conjugate line segments in the SAR image.

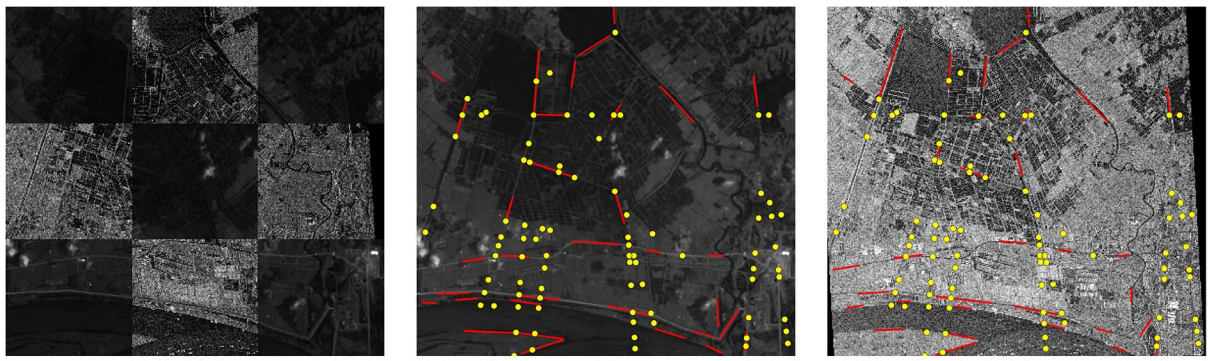

(a) (b) (c)

Fig. 15. (a) Chessboard overlay for Data Set 5. (b) Final conjugate line segments in the optical image. (c) Final conjugate line segments in the SAR image.

TABLE III
QUANTITATIVE RESULTS OF THE PROPOSED METHOD

| Image Pair | $RMSE_{all}^{*}$ | $RMSE_{LOO}^{*}$ | $P_{quad}$ | $BPP(2)$ |
|---|---|---|---|---|
| **Dataset1** | 0.832 | 0.820 | 0.492 | 0.246 |
| **Dataset2** | 1.240 | 1.269 | 0.486 | 0.328 |
| **Dataset3** | 0.985 | 1.1093 | 0.320 | 0.249 |
| **Dataset4** | 0.724 | 0.954 | 0.435 | 0.125 |
| **Dataset5** | 1.016 | 1.057 | 0.132 | 0.323 |

From the preceding experiments, we can see that the MI, improved SIFT, and MIHT methods seem ineffective. For the MI-based method, the reasons leading to their failure may be as follows. First, the MI-based method involves a careful selection of joint histogramming technique. Bad joint histogram estimation may induce interpolation-induced artifact, which not only hampers the global optimization process but also limits the accuracy [48], [49]. Second, the presence of local optima makes the function optimization a tedious task [2]. Third, the

TABLE IV
QUANTITATIVE COMPARISONS ON THE EXPERIMENT DATA SETS

| | *MI* | *Improved SIFT* | *MIHT* | *Proposed* | *Proposed+MI* |
|---|---|---|---|---|---|
| **Dataset1** | 0.803 | / | 8.290 | 0.832 | 0.653 |
| **Dataset2** | / | / | 15.938 | 1.240 | 1.032 |
| **Dataset3** | 1.182 | / | 14.349 | 0.985 | 0.738 |
| **Dataset4** | 2.013 | / | 3.480 | 0.724 | 0.564 |
| **Dataset5** | 1.236 | / | / | 1.016 | 0.858 |

initial guess of registration parameters plays an important role. Given the fact that the farther away the initial guess is from the global maximum, the more local maxima the algorithm may need to overcome, and thus the more likely it is to fail [50]. For improved SIFT, the reasons may include two aspects. First, most SIFT-based approaches are designed for small-size images; thus, they are unsuitable to extremely large images and very high resolution remote sensing imagery [51], [52]. Second, although improved, SIFT have difficulty in locating and matching conjugate point features from optical and SAR images due to their intrinsic differences [53]. For MIHT, it can be applied to multisensor image registration. However, there are three limitations. It needs a large number of primitives to estimate transformation parameters. Moreover, if correct corresponding line segments are rare while outliers are numerous in the detection procedure, the MIHT method may yield a wrong transformation model. In addition, the affine-based transformation may not be sufficient to model the deformation between multisensor images under certain conditions. However, when a more sophisticate model is adopted, the parameter solving can be more complex and time consuming. On the contrary, the proposed iterative line extraction and VSPM can be robust and practical for both high- and medium-resolution images. The comparison results demonstrate that the proposed method is more robust and accurate for the optical-to-SAR image registration.

Although the proposed method has achieved good results, the performance of the proposed method is affected by detected line segments. For Data Set 4, extracted line segments are relatively long and robust, and corresponding point pairs are uniformly distributed in the images. Thus, high matching accuracy is achieved. However, for Data Set 2, although more line segments are extracted and matched, some line pairs do not exactly correspond to each other. One of the main reasons behind this may be the great illumination difference between the optical and SAR images on buildings and roads. Thus, less control points are obtained, and the matching accuracy degrades. For Data Set 5, it is a complicated matching case due to the high scale and acquisition time differences. Some short line segments are not robust enough, whereas most line segments are well extracted. The result demonstrates the applicability of our proposed method to medium-/low-resolution image registration.

*Degraded Comparison:* In this part, comparison is limited to the fine level. Coarse registration is done by our proposed method. The performances of different approaches are listed in Table IV. It is worth mentioning that the proposed+MI method means using the MI method for further registration after performing the proposed fine registration.

Considering the obtained results in Table IV, it is easy to see that the MI and MIHT methods have better results than those without coarse registration. However, the improved SIFT method still fails to find conjugate features. Although the performance of the MIHT method improves, the matching accuracy is not satisfactory. Although MI has achieved results comparable with our proposed method for Data Set 3 and Data Set 5, the computation time of MI far overweighs that of the proposed method, which is one distinct drawback of MI. For Data Set 1, we can see that MI outperforms the proposed method. The reason is that localization error of the detected line segment end points affects the final registration result. From this point, in the case when line segments are poorly extracted, the proposed fine registration procedure can be replaced by MI. Furthermore, we can see that the proposed+MI method shows the highest matching accuracy among compared methods. Thus, to achieve better matching result, we can adopt a three-step matching procedure: coarse registration using iterative line segments detection and matching, fine registration using conjugate line intersections, and accurate registration using MI.

## V. CONCLUSION

This paper has reported a new automatic feature-based registration method for optical and SAR images. Iterative strategy involving "reexacting" and "rematching" mechanism is applied to enhance feature extraction and matching performance. Line intersections are chosen as matching primitives, and an improved point correspondence method, which is called VSPM, is proposed. Furthermore, a multilevel strategy is adopted to provide coarse-to-fine registration. Experiments have shown that our method is suitable for high- and medium-resolution optical-to-SAR image registration. Since the proposed method uses line intersections as matching primitive, it can obtain satisfactory results when linear features are abundant. On the other hand, when applied to mountainous and coastal areas without salient straight linear features, the registration would be not that robust.

Future work includes incorporating multifeatures (curves, regions) and intensity for more robust registration for areas without straight line features. Meanwhile, it is to be hoped that this paper can be also extended to other multisensor imagery registration. The main difference relies on the feature extraction techniques for extracting robust line segments.

## REFERENCES

[1] L. G. Brown, "A survey of image registration techniques," *Comput. Surveys*, vol. 24, no. 4, pp. 325–376, Dec. 1992.
[2] H. M. Chen, P. K. Varshney, and M. K. Arora, "Performance of mutual information similarity measure for registration of multitemporal remote sensing images," *IEEE Trans. Geosci. Remote Sens.*, vol. 41, no. 11, pp. 2445–2454, Nov. 2003.
[3] Y. F. Ban and A. Jacob, "Object-based fusion of multitemporal multiangle ENVISAT ASAR and HJ-1B multispectral data for urban land-cover mapping," *IEEE Trans. Geosci. Remote Sens.*, vol. 51, no. 4, pp. 1998–2006, Apr. 2013.
[4] D. Brunner, G. Lemoine, L. Bruzzone, and H. Greidanus, "Building height retrieval from VHR SAR imagery based on an iterative simulation and matching technique," *IEEE Trans. Geosci. Remote Sens.*, vol. 48, no. 3, pp. 1487–1504, Mar. 2010.

[5] Q. Li, B. H. Fu, and Y. F. Dong, "Registration of radar and optical satellite images using multiscale filter technique and information measure," in *Geoscience and Remote Sensing New Achievements*, Rijeka, Croatia: Intech, Feb. 2010, pp. 457–475.

[6] T. D. Hong and R. A. Schowengerdt, "A robust technique for precise registration of radar and optical satellite images," *Photogramm. Eng. Remote Sens.*, vol. 71, no. 5, pp. 585–593, May 2005.

[7] S. Suri and P. Reinartz, "Mutual-information-based registration of TerraSAR-X and Ikonos imagery in urban areas," *IEEE Trans. Geosci. Remote Sens.*, vol. 48, no. 2, pp. 939–949, Feb. 2010.

[8] M. A. Siddique, M. S. Sarfraz, D. Bornemann, and O. Hellwich, "Automatic registration of SAR and optical images based on mutual information assisted Monte Carlo," in *Proc. IEEE IGARSS*, Munich, Germany, Jul. 22–27, 2012, pp. 1813–1816.

[9] P. Reinartz, R. Muller, P. Schwind, S. Suri, and R. Bamler, "Orthorectification of VHR optical satellite data exploiting the geometric accuracy of TerraSAR-X data," *ISPRS J. Photogramm. Remote Sens.*, vol. 66, no. 1, pp. 124–132, Jan. 2011.

[10] L. X. Shu, T. N. Tan, M. Tang, and C. H. Pan, "A novel registration method for SAR and SPOT images," in *Proc. IEEE ICIP*, Sep. 2005, vol. 2, pp. 213–216.

[11] J. Inglada and A. Giros, "On the possibility of automatic multisensor image registration," *IEEE Trans. Geosci. Remote Sens.*, vol. 42, no. 10, pp. 2104–2120, Oct. 2004.

[12] W. Shi, F. Z. Su, R. R. Wang, and J. F. Fan, "A visual circle based image registration algorithm for optical and SAR imagery," in *Proc. IEEE IGARSS*, Munich, Germany, Jul. 22–27, 2012, pp. 2109–2112.

[13] M. Hasan, M. R. Pickering, and X. P. Jia, "Robust automatic registration of multimodal satellite images using CCRE with partial volume interpolation," *IEEE Trans. Geosci. Remote Sens.*, vol. 50, no. 10, pp. 4050–4061, Oct. 2012.

[14] W. Li and H. Leung, "A maximum likelihood approach for image registration using control point and intensity," *IEEE Trans. Image Process.*, vol. 13, no. 8, pp. 1115–1127, Aug. 2004.

[15] S. H. Wang, H. J. You, and K. Fu, "BFSIFT: A novel method to find feature matches for SAR image registration," *IEEE Geosci. Remote Sens. Lett.*, vol. 9, no. 4, pp. 649–653, Jul. 2012.

[16] M. G. Gong, S. M. Zhao, L. C. Jiao, D. Y. Tian, and S. Wang, "A novel coarse-to-fine scheme for automatic image registration based on SIFT and mutual information," *IEEE Trans. Geosci. Remote Sens.*, vol. 52, no. 7, pp. 4328–4338, Jul. 2014.

[17] A. Wong and D. A. Clausi, "AISIR: Automated inter-sensor/inter-band satellite image registration using robust complex wavelet feature representations," *Pattern Recognit. Lett.*, vol. 31, no. 10, pp. 1160–1167, Jul. 2010.

[18] A. Wong, "An adaptive Monte Carlo approach to phase-based multimodal image registration," *IEEE Trans. Inf. Technol. Biomed.*, vol. 14, no. 1, pp. 173–179, Jan. 2010.

[19] M. A. Ali and D. A. Clausi, "Automatic registration of SAR and visible band remote sensing images," in *Proc. IEEE IGARSS*, 2002, vol. 3, pp. 1331–1333.

[20] G. Hong and Y. Zhang, "Wavelet-based image registration technique for high-resolution remote sensing images," *Comput. Geosci.*, vol. 34, no. 12, pp. 1708–1720, Dec. 2008.

[21] B. Fan, C. L. Huo, C. H. Pan, and Q. Q. Kong, "Registration of optical and SAR satellite images by exploring the spatial relationship of the improved SIFT," *IEEE Geosci. Remote Sens. Lett.*, vol. 10, no. 4, pp. 657–661, Jul. 2013.

[22] L. Huang and Z. Li, "Feature-based image registration using the shape context," *Int. J. Remote Sens.*, vol. 31, no. 8, pp. 2169–2177, Apr. 2010.

[23] H. Cheng, S. Zheng, Q. Z. Yu, J. W. Tian, and L. Jian, "Matching of SAR images and optical images based on edge feature extracted via SVM," in *Proc. ICSP*, Aug. 31–Sep. 4, 2004, vol. 2, pp. 930–933.

[24] C. Pan, Z. Zhang, H. Yan, G. Wu, and S. Ma, "Multisource data registration based on NURBS description of contours," *Int. J. Remote Sens.*, vol. 29, no. 2, pp. 569–591, Jan. 2008.

[25] H. Li, B. S. Manjunath, and S. K. Mitra, "A contour-based approach to multisensor image registration," *IEEE Trans. Image Process.*, vol. 4, no. 3, pp. 320–334, Mar. 1995.

[26] A. F. Habib and R. I. Alruzouq, "Semi-automatic registration of multi-source satellite imagery with varying geometric resolutions," *Photogramm. Eng. Remote Sens.*, vol. 71, no. 3, pp. 325–332, Mar. 2005.

[27] Z. Hu, "Line based SAR and optical image automatic registration method," *Proc. CCPR*, Chongqing, China, Oct. 21–23, 2010, pp. 1–5.

[28] P. Dare and I. Dowman, "An improved model for automatic feature-based registration of SAR and SPOT images," *ISPRS J. Photogramm. Remote Sens.*, vol. 56, no. 1, pp. 13–28, Jun. 2001.

[29] A. F. Habib and R. I. Alruzouq, "Line-based modified iterated Hough transform for automatic registration of multi-source imagery," *Photogramm. Rec.*, vol. 19, no. 105, pp. 5–21, Mar. 2004.

[30] Z. Xiong and Y. Zhang, "A novel interest-point-matching algorithm for high-resolution satellite images," *IEEE Trans. Geosci. Remote Sens.*, vol. 47, no. 12, pp. 4189–4200, Dec. 2009.

[31] G. J. Wen, J. J. Lv, and W. X. Yu, "A high-performance feature-matching method for image registration by combining spatial and similarity information," *IEEE Trans. Geosci. Remote Sens.*, vol. 46, no. 4, pp. 1266–1277, Apr. 2008.

[32] Z. X. Liu, J. B. An, and Y. Jing, "A simple and robust feature point matching algorithm based on restricted spatial order constraints for aerial image registration," *IEEE Trans. Geosci. Remote Sens.*, vol. 50, no. 2, pp. 514–527, Feb. 2012.

[33] M. Carcassoni and E. R. Hancock, "Spectral correspondence for point pattern matching," *Pattern Recognit.*, vol. 36, no. 1, pp. 193–204, Jan. 2003.

[34] R. Gioi, J. Jakubowicz, J. M. Morel, and G. Randall, "LSD: A fast line segment detector with a false detection control," *IEEE Trans. Pattern Anal. Mach. Intell.*, vol. 32, no. 4, pp. 722–732, Apr. 2010.

[35] T. Esch *et al.*, "Characterization of land cover types in TerraSAR-X images by combined analysis of speckle statistics and intensity information," *IEEE Trans. Geosci. Remote Sens.*, vol. 49, no. 6, pp. 1911–1925, Jun. 2011.

[36] J. S. Lee, "Digital image enhancement and noise filtering by use of local statistics," *IEEE Trans. Pattern Anal. Mach. Intell.*, vol. PAMI-2, no. 2, pp. 165–168, Mar. 1980.

[37] P. L. Shui and D. Cheng, "Edge detector of SAR images using Gaussian-Gamma-shaped bi-windows," *IEEE Geosci. Remote Sens. Lett.*, vol. 9, no. 5, pp. 846–850, Sep. 2012.

[38] L. Shapiro and J. Brady, "Feature-based correspondence: An eigenvector approach," *Image Vis. Comput.*, vol. 10, no. 5, pp. 283–288, Jun. 1991.

[39] N. Ahuja, "Dot pattern processing using Voronoi neighborhoods," *IEEE Trans. Pattern Anal. Mach. Intell.*, vol. PAMI-4, no. 3, pp. 336–343, May 1982.

[40] H. Lombaert, L. Grady, J. R. Polimeni, and F. Cheriet, "Fast brain matching with spectral correspondence," in *Information Processing in Medical Imaging*. Berlin, Germany: Springer-Verlag, 2011, pp. 660–673.

[41] T. C. Henderson, E. E. Triendl, and R. Winter, "Edge- and shape-based geometric registration," *IEEE Trans. Geosci. Remote Sens.*, vol. GE-23, no. 3, pp. 334–342, May 1985.

[42] Y. Zhang, Y. Guo, and Y. F. Gu, "Robust feature matching and selection methods for multisensor image registration," in *Proc. IEEE IGARSS*, Cape Town, South Africa, Jul. 12–17, 2009, vol. 3, pp. III 255–III 258.

[43] Y. Wu and M. Yang, "A multi-sensor remote sensing image matching method based on SIFT operator and CRA similarity measure," in *Proc. ISIE*, Wuhan, China, Aug. 20–21, 2011, pp. 115–118.

[44] E. Coiras, J. Santamaria, and C. Miravet, "Segment-based registration technique for visual-infrared images," *Opt. Eng.*, no. 39, vol. 1, pp. 282–289, Jan. 2000.

[45] M. Izadi and P. Saeedi, "Robust weighted graph transformation matching for rigid and nonrigid image registration," *IEEE Trans. Image Process.*, vol. 21, no. 10, pp. 4369–4382, Oct. 2012.

[46] L. M. G. Fonseca and B. S. Manjunath, "Registration techniques for multisensor remotely sensed imagery," *Photogramm. Eng. Remote Sens.*, vol. 62, no. 9, pp. 1049–1056, Sep. 1996.

[47] H. Gonçalves, J. A. Gonçalves, and L. Corte-Real, "Measures for an objective evaluation of the geometric correction process quality," *IEEE Geosci. Remote Sens. Lett.*, vol. 6, no. 2, pp. 292–296, Apr. 2009.

[48] J. Tsao, "Interpolation artifacts in multimodality image registration based on maximization of mutual information," *IEEE Trans. Geosci. Remote Sens.*, vol. 22, no. 7, pp. 854–864, Jul. 2003.

[49] J. Inglada, V. Muron, D. Pichard, and T. Feuvrier, "Analysis of artifacts in subpixel remote sensing image registration," *IEEE Trans. Geosci. Remote Sens.*, vol. 45, no. 1, pp. 254–264, Jan. 2007.

[50] A. A. Cole-Rhodes, K. L. Johnson, J. LeMoigen, and I. Zavorin, "Multiresolution registration of remote sensing imagery by optimization of mutual information using a stochastic gradient," *IEEE Trans. Image Process.*, vol. 12, no. 12, pp. 1495–1511, Dec. 2003.

[51] C. L. Huo, C. H. Pan, L. G. Huo, and Z. X. Zhou, "Multilevel SIFT matching for large-size VHR image registration," *IEEE Geosci. Remote Sens. Lett.*, vol. 9, no. 2, pp. 171–175, Mar. 2012.

[52] L. Wang, Z. Niu, C. Y. Wu, R. W. Xie, and H. B. Huang, "A robust multisource image automatic registration system based on the SIFT descriptor," *Int. J. Remote Sens.*, vol. 33, no. 12, pp. 3850–3869, Jun. 2012.

[53] Q. L. Li, G. Y. Wang, J. G. Liu, and S. B. Chen, "Robust scale-invariant feature matching for remote sensing image registration," *IEEE Geosci. Remote Sens. Lett.*, vol. 6, no. 2, pp. 287–291, Apr. 2009.

**Haigang Sui** received the B.S. degree and the Ph.D. degree in photogrammetry and remote sensing from Wuhan University, Wuhan, China, in 1996 and 2002, respectively.

He is currently a Professor with the State Key Laboratory of Information Engineering in Surveying, Mapping and Remote Sensing, Wuhan University. His major research interests include change detection of remote sensing, target recognition, and disaster analysis.

**Chuan Xu** received the B.S. degree from Huazhong Agricultural University, Wuhan, China, in 2006 and the M.S. and Ph.D. degrees from Wuhan University, Wuhan, in 2009 and 2013, respectively.

She is currently a Postdoctorate Candidate with the State Key Laboratory of Information Engineering in Surveying, Mapping and Remote Sensing, Wuhan University. Her research interests include algorithm development and application for synthetic aperture radar image segmentation, classification, image registration, and target recognition.

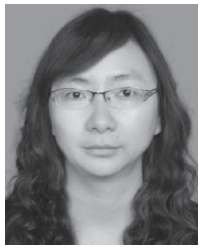

**Junyi Liu** received the B.S. degree in sciences and techniques of remote sensing and the Ph.D. degree in photogrammetry and remote sensing from Wuhan University, Wuhan, China, in 2002 and 2008, respectively.

She is currently an Associate Professor with the State Key Laboratory of Information Engineering in Surveying, Mapping and Remote Sensing, Wuhan University. Her research interests include algorithm development and application for synthetic aperture radar image segmentation, image registration, and change detection.

**Feng Hua** received the B.S. degree from Hubei University, Wuhan, China, in 2012 and the M.S. degree from Wuhan University, Wuhan, in 2015.

She is currently with the State Key Laboratory of Information Engineering in Surveying, Mapping and Remote Sensing, Wuhan University. Her research interests include algorithms and applications for image registration and target recognition.